COMPUTER RESEARCH AND MODELING
2026 VOL. 18 NO. 2 P. 399–421
DOI: 10.20537/2076-7633-2026-18-2-399-421

Ки&М

MODELS IN PHYSICS AND TECHNOLOGY

UDC: 004.94 + 666.192

Simulation of laser polishing for fused quartz

Yu. V. Nikityuk[1,a], L. N. Marchenko[1,3,b], A. N. Serdyukov[1,c], Iu. V. Bruttan[2,d]

[1]Francisk Skorina Gomel State University,
104 Sovetskaya st., Gomel, 246028, Belarus
[2]Pskov State University,
2 Lenin sq., Pskov, 180000, Russia
[3]Sofia Kovalevskaya Northwestern Center for Mathematical Research, Pskov State University,
2, Lenin sq., Pskov, 180000, Russia

E-mail: [a] nikitjuk@gsu.by, [b] lmarchenko@gsu.by, [c] serdukov1944@gmail.com, [d] bruttan@mail.ru

Received 22.01.2026, after completion — 06.03.2026.
Accepted for publication 13.03.2026.

Laser polishing is a promising technology for the finishing of fused quartz (fused silica or quartz glass) products, enabling the removal of subsurface defects induced by mechanical processing. However, the complexity and nonlinearity of the physical processes occurring during laser irradiation complicate the selection of optimal technological parameters. The present paper aims to develop, comparatively analyze, and apply high-precision predictive models for forecasting and optimizing the key performance indicators of the laser polishing process for quartz glass. A verified finite element model implemented in the ANSYS software environment produced a dataset of temperature and stress fields for various combinations of process parameters. This dataset was used to develop and validate four types of predictive models: Polynomial Regression, a Fuzzy Logic System, an Adaptive Neuro-Fuzzy Inference System (ANFIS), and a Multilayer Perceptron (MLP) neural network. The models' quality was evaluated on a test set using the statistical metrics MAE, RMSE, MAPE, R^2, and R^2_{Adj}. A comparative analysis of the models revealed the significant superiority of the MLP neural network, which demonstrated the highest prediction accuracy for all output parameters, achieving Adjusted R^2 (R^2_{Adj}) values above 0.97 and a Mean Absolute Percentage Error (MAPE) in the range of 0.7–2.8 %. This model was effectively utilized as a surrogate function in combination with a genetic algorithm to successfully identify the optimal process parameters. The constructed MLP neural network model functions as a reliable and high-precision tool, facilitating both prediction and the optimization of fused quartz polishing outcomes using a CO_2 laser. This approach effectively approximates the complex nonlinear dependencies inherent in the process and can serve as a foundation for developing intelligent control and optimization systems for this technology.

Keywords: laser polishing, ANSYS, modeling, regression, fuzzy logic system, ANFIS, neural network model, optimization

Citation: *Computer Research and Modeling*, 2026, vol. 18, no. 2, pp. 399–421.

КОМПЬЮТЕРНЫЕ ИССЛЕДОВАНИЯ
И МОДЕЛИРОВАНИЕ 2026 Т. 18 № 2 С. 399–421
DOI: 10.20537/2076-7633-2026-18-2-399-421

Ки&М

МОДЕЛИ В ФИЗИКЕ И ТЕХНОЛОГИИ

УДК: 004.94 + 666.192

Моделирование лазерной полировки кварцевого стекла

Ю. В. Никитюк[1,a], Л. Н. Марченко[1,3,b], А. Н. Сердюков[1,c], Ю. В. Бруттан[2,d]

[1]Гомельский государственный университет имени Франциска Скорины,
Беларусь, 246028, г. Гомель, ул. Советская, д. 104
[2]Псковский государственный университет,
Россия, 180000, г. Псков, пл. Ленина, д. 2
[3]Научно-образовательный математический центр «Северо-Западный центр математических исследований имени Софьи Ковалевской» Псковского государственного университета,
Россия, 180000, г. Псков, пл. Ленина, д. 2

E-mail: [a] nikitjuk@gsu.by, [b] lmarchenko@gsu.by, [c] serdukov1944@gmail.com, [d] bruttan@mail.ru

Получено 22.01.2026, после доработки — 06.03.2026.
Принято к публикации 13.03.2026.

Лазерная полировка является перспективной технологией финишной обработки изделий из кварцевого стекла, позволяющей устранять дефекты подповерхностного слоя, возникающие при механической обработке. Однако сложность и нелинейность физических процессов, протекающих при лазерном воздействии, затрудняют подбор оптимальных технологических режимов. Целью данной статьи является разработка, сравнительный анализ и применение высокоточных прогностических моделей для предсказания и оптимизации основных показателей процесса лазерной полировки кварцевого стекла. На основе верифицированной конечно-элементной модели, реализованной в среде ANSYS, был сгенерирован набор данных о температурных полях и полях напряжений при различных сочетаниях технологических параметров. Этот набор данных использовался для построения и верификации четырех типов прогностических моделей: полиномиальной регрессии, нечеткой системы вывода (Fuzzy Logic), адаптивной нейро-нечеткой системы (ANFIS) и нейронной сети типа многослойный персептрон (MLP). Качество моделей оценивалось на тестовой выборке с использованием статистических метрик MAE, RMSE, MAPE, R^2, R^2_{Adj}. Сравнительный анализ моделей показал значительное превосходство нейросетевой модели MLP, которая продемонстрировала наивысшую точность прогнозирования для всех выходных параметров, достигнув значений скорректированного коэффициента детерминации (R^2_{Adj}) выше 0,97 и средней абсолютной процентной ошибки (MAPE) в диапазоне 0,7–2,8 %. Использование этой модели в качестве суррогатной функции совместно с генетическим алгоритмом позволило успешно определить оптимальные технологические параметры. Разработанная нейросетевая модель MLP является надежным и высокоточным инструментом не только для прогнозирования, но и для оптимизации результатов лазерной полировки кварцевого стекла CO_2-лазером. Она способна эффективно аппроксимировать сложные нелинейные зависимости в процессе и может служить основой для создания интеллектуальных систем управления и оптимизации данной технологии.

Ключевые слова: лазерная полировка, ANSYS, моделирование, регрессия, нечеткая система вывода, ANFIS, нейросетевая модель, оптимизация

Introduction

The unique combination of physicochemical properties, namely high thermal resistance, chemical inertness, mechanical strength, and broad optical transparency, makes fused quartz an indispensable material across various fields of science and technology, such as laser optics, microelectronics, and the aerospace industry. A critical challenge in this area is achieving high-quality surface finishing of fused quartz components, which has traditionally been accomplished by mechanical polishing methods [Арбузов, 2008]. Nonetheless, mechanical processing inevitably leads to the formation of a defective subsurface layer, comprising microcracks, scratches, and residual stresses. These defects critically degrade the operational performance of the components by acting as initiation sites for laser radiation absorption, ultimately leading to a reduction in the laser-induced damage threshold (LIDT).

An effective noncontact alternative is the technology of laser polishing, which relies on the local melting of a thin surface layer by CO_2 laser radiation. The influence of surface tension forces in the resulting micromelt pool leads to the smoothing of the original microtopography, facilitating the attainment of the desired roughness level and the efficient elimination of defects from prior processing [Sysoev, 2003; Hildebrand et al., 2011; Hildebrand et al., 2012; Шершнев и др., 2015; Достанко и др., 2020; Емельянов и др., 2022; Lu et al., 2024]. The laser polishing process represents a complex, multiparametric system characterized by nonlinear interdependencies between the process parameters and the final quality characteristics. Accurate predictive models are essential for the optimization of this process. A theoretical model in three dimensions for the photochemical polishing of quartz glass is presented in [Kanevskii et al., 2024], which forecasts surface evolution based on the polarization state of the incident light. This study demonstrates that linearly polarized light results in the creation of grooved textures, whereas unpolarized light yields flatter surfaces. In [Бибичева и др., 2022], femtosecond pulses from an ytterbium fiber laser (1030 nm, 20–48 nJ, 100 kHz, NA 0.65) were studied; these pulses generate self-organized subwavelength periodic nanostructures with a period of 250 nanometers, and the minimum pulse energy required for structure formation without ablation was determined. The investigation of computer modeling of thermoelastic fields, alongside experimental verification using a CO_2 laser to analyze controlled thermal cleavage of quartz, was conducted in [Serdyukov et al., 2012].

The laser polishing process is frequently simulated using experimental design and regression modeling, which have proven to be effective. A quadratic model was developed in [Rosa et al., 2014] to optimize the laser polishing process, accounting for the initial surface topography and laser parameters, including power, feed rate, and overlap. The model accurately predicts surface quality and determines optimal processing parameters that can decrease roughness by as much as 85 % while enhancing polishing efficiency.

The finite element method (FEM) is widely used in research on laser processing of brittle nonmetallic materials [Nikityuk et al., 2025; Serdyukov et al., 2010; Serdyukov et al., 2012].

An analysis of existing laser polishing models, including regression-based approaches, is provided by [Mohajerani et al., 2018]. It is observed that most models are based on simplifications and fail to fully describe the thermophysical processes, especially under complex geometries and variable processing conditions, which represent latent nonlinear dependencies.

The significant computational cost of finite element modeling limits the possibilities for rapid analysis and optimization of process parameters. To overcome this limitation, there is an increasing focus on employing data-driven intelligent models derived from data obtained via finite element analysis. These models can significantly reduce computational expenses.

The study by [Solheid et al., 2022] integrates experimental design with the development of linear regression models and neural network modeling. The authors note that, while regression models provide satisfactory results, they are outperformed by neural networks in accurately describing the complex relationships between laser processing parameters and surface quality.

This approach demonstrates the effectiveness of artificial neural networks, fuzzy systems, and neuro-fuzzy systems in exploring laser processing phenomena. Such methods are widely adopted across various domains for modeling real-world processes with limited training data [Марченко и др., 2024]. The application of genetic algorithms offers a highly efficient approach for identifying the optimal process parameters [Jiang et al., 2020; Kharche, Patil, 2024; Nisar, 2025; Nikityuk et al., 2022a; Nikitjuk, Serdyukov, 2023; Nikityuk et al., 2024].

Despite significant progress in the modeling of laser polishing of quartz glass, a literature review reveals several unresolved issues and underexplored aspects. Existing studies generally focus on developing models that adequately describe isolated physical phenomena (e. g., heat transfer, stress formation) or on applying specific machine learning methods to approximate dependencies. However, a comprehensive comparative analysis of various classes of predictive models — including polynomial, fuzzy, neuro-fuzzy, and deep neural networks — applied to the laser polishing of brittle nonmetallic materials remains fragmented in current research. The selection of the most effective and accurate approach for the simultaneous prediction of the entire complex of thermomechanical characteristics (temperatures and stresses at various time stages) remains an open question, particularly given the pronounced nonlinearity and multifactorial nature of the process.

Furthermore, most existing models serve primarily analytical purposes. Their direct integration into an optimization loop for the automated determination of processing parameters — balancing throughput (processing speed) and quality (minimization of residual stresses) — has not been sufficiently investigated. Therefore, it is necessary to develop a methodology that combines a high-precision predictive model with a modern heuristic multiobjective optimization algorithm.

Consequently, the aim of this study is the development, comparative analysis, and practical application of AI-based predictive models for the laser polishing of quartz glass. The work addresses the following objectives:

1. To conduct a systematic comparison of the accuracy and interpretability of polynomial regression, fuzzy logic, Adaptive Neuro-Fuzzy Inference System (ANFIS), and Multi-Layer Perceptron (MLP) models in predicting temperature and residual stress fields.

2. To identify the most effective model capable of accurately approximating complex nonlinear relationships between processing parameters and output characteristics based on statistical metrics.

3. To integrate the superior model with a genetic algorithm to solve the critical engineering problem of multiobjective optimization of laser polishing regimes.

This research will provide fundamental insights into the relative effectiveness of different modeling approaches and yield a practical toolkit for process engineers. This contribution aims to reduce the need for costly empirical trials and establish the foundations for intelligent control systems in high-precision laser processing.

Finite element model

The process of simulating the laser heating of quartz glass was conducted following the schematic outlined in Fig. 1. The laser beam is designated as 1, while the fused quartz is labeled 2. The illustration employs linear representations with arrows to denote the movement directions of the laser beam in relation to the workpiece. The letter S represents the scanning step of the elliptical laser beam 1.

The simulation of temperature and stress fields was performed in the ANSYS finite element analysis software using the APDL programming language. The calculations employed a plate with

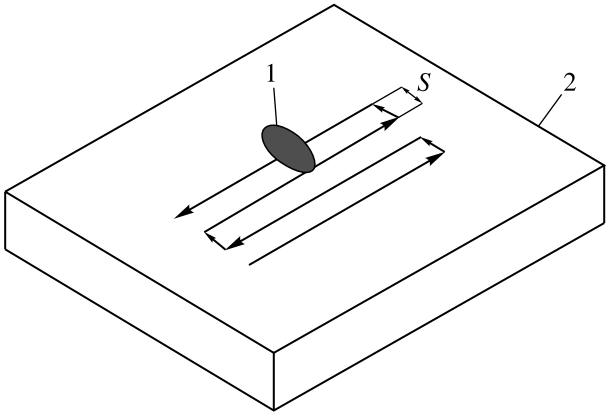

Figure 1. Laser beam scanning pattern in the processing zone: 1 — laser beam spot; 2 — quartz plate

geometric dimensions of 15 × 15 × 2 mm and a finite element model consisting of 14 400 elements. The Solid 70 element type was applied for the thermal analysis, while the Solid 185 element type was used for the structural analysis. The simulation accounted for the temperature dependence of the thermophysical properties of quartz glass [Hildebrand et al., 2011; Шершнев и др., 2015]. The mechanical behavior of quartz glass upon heating is complex: at room temperature, it behaves as an elastic and brittle material, but upon reaching the glass transition temperature, its viscosity decreases sharply. The stress relaxation effect is of significant importance for modeling the laser polishing process of quartz glass. In APDL, this material behavior was implemented using a viscoelastic model (TB, PRONY). The temperature-dependent viscosity relationship presented in [Hildebrand et al., 2011] was used to calibrate the model parameters.

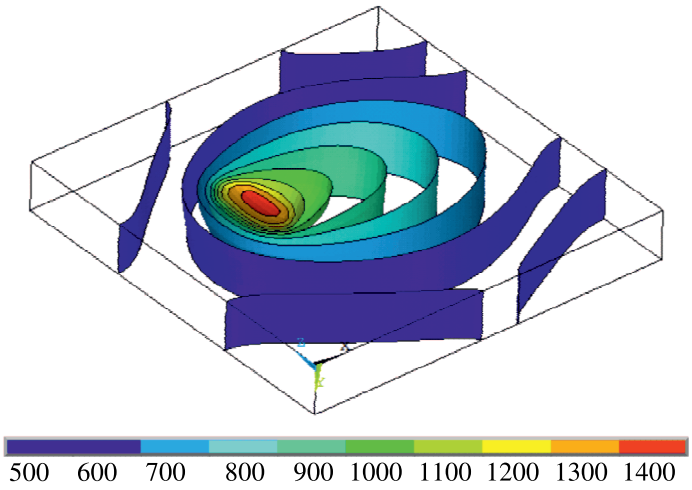

Figure 2. Temperature distribution within the volume of the processed quartz plate at the end of the laser treatment, K

Figures 2–5 illustrate the distributions of the temperature and stress fields under the following process parameters: the relative velocity module of the laser beam and the sample V = 0.002 m/s, the output power of the CO_2 laser radiation P = 30 W, the semiaxes of the elliptical laser beam cross-section A = 0.001 m, B = 0.002 m, and the scanning pitch S = 0.005 m. The scanning was conducted along the direction of the minor semiaxis of the elliptical CO_2 laser beam. The temperatures and stresses were determined at the end of the processing cycle and 1000 seconds after its completion.

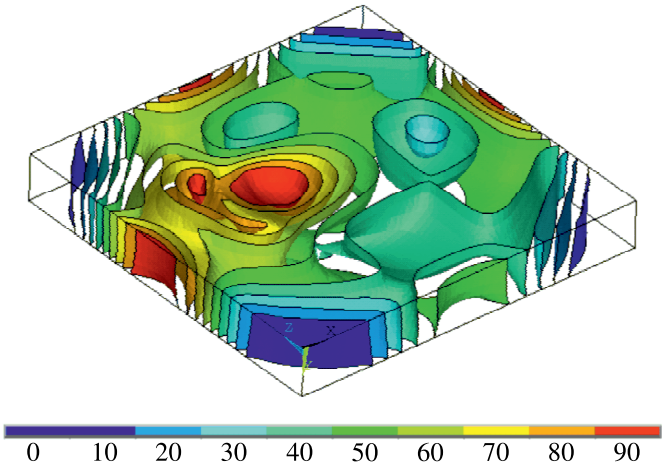

Figure 3. Distribution of von Mises equivalent stress within the volume of the processed quartz plate at the end of the laser treatment, MPa

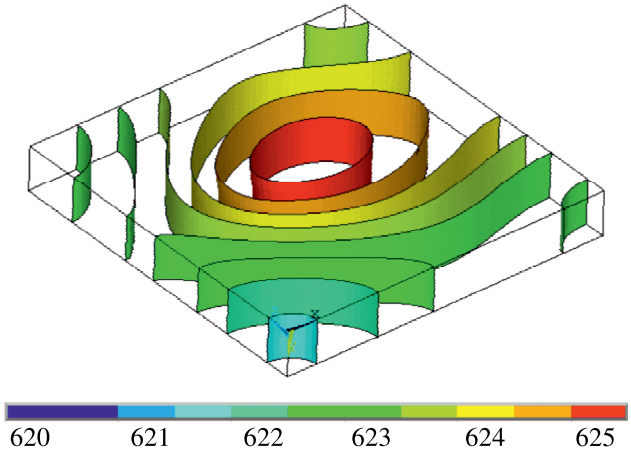

Figure 4. Temperature distribution within the volume of the processed quartz plate 1000 seconds posttreatment, K

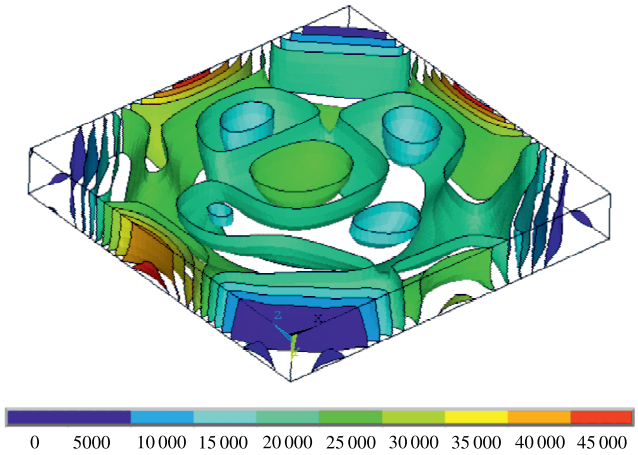

Figure 5. Distribution of von Mises equivalent stress within the volume of the processed quartz glass plate 1000 seconds posttreatment, Pa

The finite element model was verified using experimental data obtained from a CO_2 laser and an IT-3SM thermal imager. The relative error in determining the maximum temperatures on the quartz plate's surface did not surpass 5 %, indicating that the finite element modeling results align satisfactorily with the experimental data.

Regression model

A face-centered central composite design was generated in the ANSYS DesignXplorer module to define the values of five input parameters: $P1$ is the processing speed V, $P2$ is the power P of the CO_2 laser, $P3$ and $P4$ are the semiaxes A and B of the elliptical laser beam, $P5$ is the scanning pitch S (Table 1).

Table 1. Experimental design and calculation results

N	$P1$ (V), m/s	$P2$ (P), W	$P3$ (A), m	$P4$ (B), m	$P5$ (S), m	$P6$ ($T1$), K	$P7$ ($S1$), Pa	$P8$ ($T2$), K	$P9$ ($S2$), Pa
1	0.0020	65	0.0015	0.0025	0.0005	1940	2.44E+07	1021	5.57E+04
2	0.0010	65	0.0015	0.0025	0.0005	2317	2.02E+07	1633	2.20E+04
3	0.0030	65	0.0015	0.0025	0.0005	1800	1.91E+07	799	8.23E+04
4	0.0020	50	0.0015	0.0025	0.0005	1701	1.56E+07	872	5.75E+04
5	0.0020	80	0.0015	0.0025	0.0005	2155	2.97E+07	1166	4.75E+04
6	0.0020	65	0.0010	0.0025	0.0005	1988	2.50E+07	961	5.68E+04
7	0.0020	65	0.0020	0.0025	0.0005	1879	2.16E+07	1039	5.41E+04
8	0.0020	65	0.0015	0.0020	0.0005	2022	2.74E+07	991	5.77E+04
9	0.0020	65	0.0015	0.003	0.0005	1856	1.98E+07	1027	5.51E+04
10	0.0020	65	0.0015	0.0025	0.00025	1942	2.47E+07	1021	5.69E+04
11	0.0020	65	0.0015	0.0025	0.00075	1938	2.37E+07	1021	6.53E+04
12	0.0010	50	0.0010	0.0020	0.00075	2108	2.16E+07	1255	3.03E+04
13	0.0030	50	0.0010	0.0020	0.00025	1742	1.62E+07	653	8.09E+04
14	0.0010	80	0.0010	0.0020	0.00025	2701	2.40E+07	1736	2.40E+04
15	0.0030	80	0.001	0.0020	0.00075	2184	3.57E+07	838	8.76E+04
16	0.0010	50	0.002	0.0020	0.00025	2011	1.80E+07	1373	2.40E+04
17	0.0030	50	0.0020	0.0020	0.00075	1604	1.67E+07	699	8.02E+04
18	0.0010	80	0.0020	0.0020	0.00075	2639	2.16E+07	1899	2.70E+04
19	0.003	80	0.0020	0.002	0.00025	2032	3.28E+07	907	8.69E+04
20	0.0010	50	0.0010	0.003	0.00025	1944	1.73E+07	1287	2.33E+04
21	0.0030	50	0.0010	0.003	0.00075	1523	1.61E+07	667	7.88E+04
22	0.0010	80	0.0010	0.003	0.00075	2541	2.10E+07	1779	2.71E+04
23	0.0030	80	0.0010	0.003	0.00025	1937	2.66E+07	857	8.13E+04
24	0.0010	50	0.002	0.003	0.00075	1930	1.45E+07	1412	2.58E+04
25	0.0030	50	0.002	0.003	0.00025	1469	1.64E+07	714	7.87E+04
26	0.0010	80	0.0020	0.003	0.00025	2519	1.91E+07	1953	2.22E+04
27	0.0030	80	0.0020	0.003	0.00075	1847	2.30E+07	931	8.50E+04

The output parameters included the maximum temperature $T1$ ($P6$) and the maximum von Mises equivalent stress $S1$ ($P7$) in the quartz plate at the end of the laser treatment, as well as the maximum temperature $T2$ ($P8$) and the maximum von Mises equivalent stress $S2$ ($P9$) measured 1000 seconds post-treatment.

The estimated regression models for the dependencies of the output parameters $T1$, $S1$, $T2$, $S2$ on the input parameters V, P, A, B, S, at a significance level of 0.05, are as follows:

$$T1 = e^{Y_{T1}} - 1,$$
$$S1 = e^{Y_{S1}} - 1,$$
$$T2 = e^{Y_{T2}} - 1,$$
$$S2 = (1.305 \cdot Y_{S2} + 1)^{1/1.305} - 1,$$

where

$$Y_{T1} = 7.176 - 173.1 \cdot V + 0.01704 \cdot P + 50\,970 \cdot V^2 - 5.997 \cdot 10^{-5} P^2 -$$
$$-0.5086 \cdot V \cdot P - 18\,660 \cdot V \cdot A - 37\,650 \cdot V \cdot B - 2046 \cdot A \cdot B,$$
$$Y_{S1} = 17.07 - 99.52 \cdot A - 187.5 \cdot B - 100\,700 \cdot V^2 + 6.900 \cdot V \cdot P,$$
$$Y_{T2} = 6.532 - 725.7 \cdot V + 0.01749 \cdot P + 323.6 \cdot A + 202.3 \cdot B + 115\,100 \cdot V^2 -$$
$$-4.279 \cdot 10^{-5} \cdot P^2 - 74\,800 \cdot A^2 - 35\,340 \cdot B^2 - 1.124 \cdot V \cdot P - 8471 \cdot V \cdot A,$$
$$Y_{S2} = -443\,200 + 785\,600\,000 \cdot V + 2\,537\,000 \cdot P \cdot S.$$

The influence quantity of the input parameters V ($P1$), P ($P2$), A ($P3$), B ($P4$), S ($P5$) on the output parameters $T1$ ($P6$), $S1$ ($P7$), $T2$ ($P8$), $S2$ ($P9$) was assessed using local sensitivity coefficients (Fig. 6).

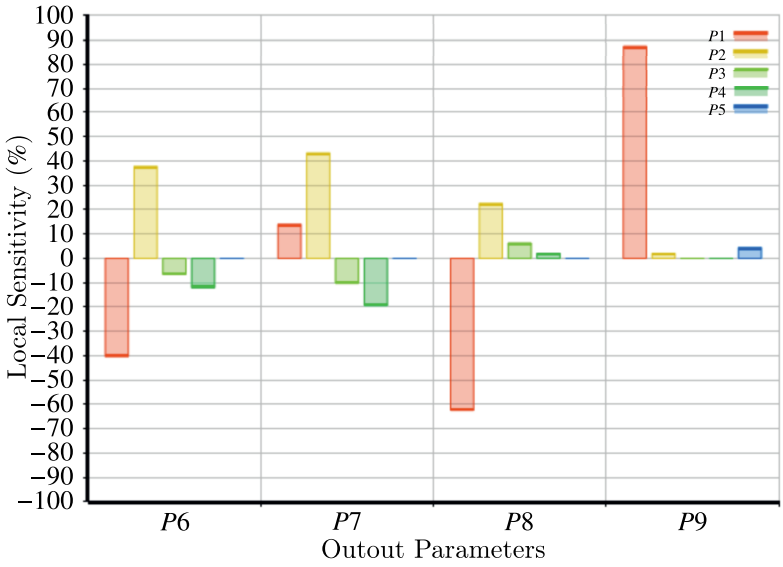

Figure 6. Diagram illustrating the local sensitivity coefficients for the laser polishing parameters of fused quartz $T1$ ($P6$), $S1$ ($P7$), $T2$ ($P8$), $S2$ ($P9$) with respect to the input parameters V ($P1$), P ($P2$), A ($P3$), B ($P4$), S ($P5$)

The maximum temperatures $T1$ ($P6$) and $T2$ ($P8$) in the processing zone are determined by the balance between the speed V ($P1$), which exhibits strong negative sensitivity, and the power P ($P2$) of the CO_2 laser, which has a comparable positive sensitivity. In contrast, the level of the maximum residual stresses $S1$ ($P7$) and $S2$ ($P9$), which are critical parameters, is dominantly influenced by the processing speed V ($P1$), demonstrating very high positive sensitivity. This indicates that high heating and subsequent cooling rates, caused by rapid processing, lead to the “freezing” of stresses. Meanwhile,

the influence of laser power P ($P2$) and beam spot geometry ($P3$ and $P4$) on the final stress level is negligible.

The approximating response surfaces for the dependencies of the output parameters $T1$ ($P6$), $S1$ ($P7$), $T2$ ($P8$), $S2$ ($P9$) on the process parameters V ($P1$), P ($P2$), A ($P3$), B ($P4$), S ($P5$), derived from the regression model, are presented in Fig. 7.

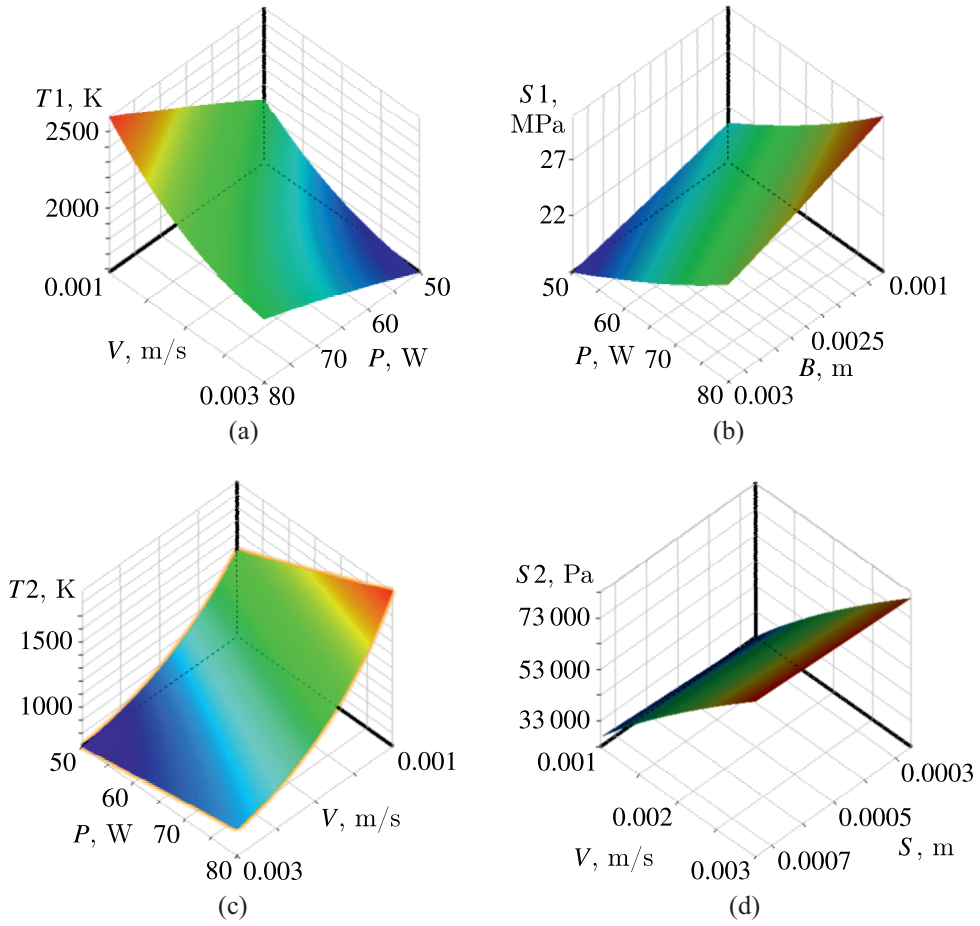

Figure 7. Output parameters vs. process parameters, obtained using the regression model: a) $T1$ ($P6$), K, vs. V ($P1$), m/s, and P ($P2$), W; b) $S1$ ($P7$), Pa, vs. P ($P2$), W, and B ($P4$), m, c) $T2$ ($P8$), K, vs. V ($P1$), m/s, and P ($P2$), W; d) $S2$ ($P9$), Pa, vs. V ($P1$), m/s, and S ($P5$), m

Fuzzy model

Fuzzy modeling of the laser polishing process for fused quartz was performed using a Mamdani-type fuzzy inference system (Fig. 8) [Штовба, 2007; Nikityuk et al., 2024]. The model was implemented with the Scikit-Fuzzy library of the Python programming language. The input parameters V ($P1$), P ($P2$), A ($P3$), B ($P4$), S ($P5$) were represented by triangular membership functions, while the output parameters $T1$ ($P6$), $S1$ ($P7$), $T2$ ($P8$), $S2$ ($P9$) were represented by Gaussian membership functions (Fig. 9).

The following linguistic variables were defined for the input and output parameters.

Input parameters: {“little” (L), “medium” (M), “high” (H)};

Output parameters: {“very little” (out1_VL), “little” (out2_L), “little-medium” (out3_LM), “medium” (out4_M), “medium-high” (out5_MH), “high” (out6_H), “very high” (out7_VH)}.

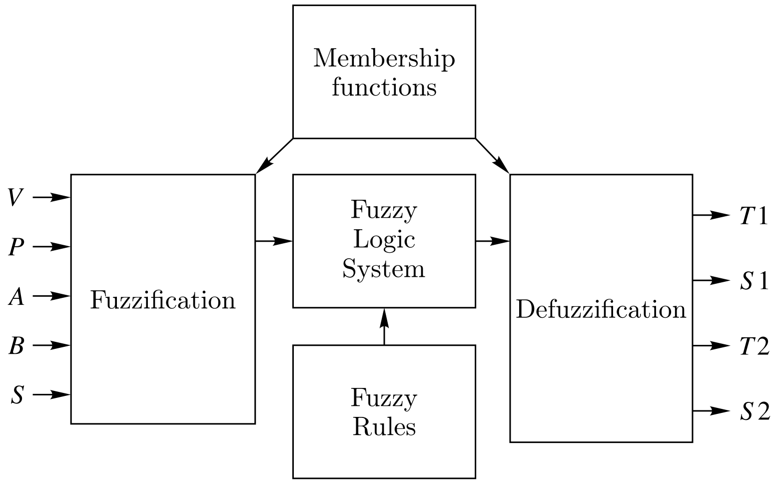

Figure 8. Structure of the fuzzy system used to simulate fused quartz laser polishing

Four rule sets for determining the four output parameters $T1$ ($P6$), $S1$ ($P7$), $T2$ ($P8$), and $S2$ ($P9$) were formulated based on the data from the computational experiment (Table 1):

```
ctrl.Rule(V['L'] & P['L'] & (B['L'] | B['M']), T1_ctrl['out3_LM']),
ctrl.Rule(V['L'] & P['L'] & B['H'], T1_ctrl['out2_L']),
ctrl.Rule(V['L'] & P['M'] & (B['L'] | B['M']), T1_ctrl['out5_MH']),
ctrl.Rule(V['L'] & P['M'] & B['H'], T1_ctrl['out4_M']),
ctrl.Rule(V['L'] & P['H'] & (B['L'] | B['M']), T1_ctrl['out6_H']),
ctrl.Rule(V['L'] & P['H'] & B['H'], T1_ctrl['out5_MH']),
ctrl.Rule(V['M'] & P['L'] & (B['L'] | B['M']), T1_ctrl['out2_L']),
ctrl.Rule(V['M'] & P['L'] & B['H'], T1_ctrl['out1_VL']),
ctrl.Rule(V['M'] & P['M'] & (B['L'] | B['M']), T1_ctrl['out3_LM']),
ctrl.Rule(V['M'] & P['M'] & B['H'], T1_ctrl['out2_L']),
ctrl.Rule(V['M'] & P['H'] & (B['L'] | B['M']), T1_ctrl['out4_M']),
ctrl.Rule(V['M'] & P['H'] & B['H'], T1_ctrl['out3_LM']),
ctrl.Rule(V['H'] & P['L'], T1_ctrl['out1_VL']),
ctrl.Rule(V['H'] & P['M'] & (B['L'] | B['M']), T1_ctrl['out2_L']),
ctrl.Rule(V['H'] & P['M'] & B['H'], T1_ctrl['out1_VL']),
ctrl.Rule(V['H'] & P['H'] & (B['L'] | B['M']), T1_ctrl['out3_LM']),
ctrl.Rule(V['H'] & P['H'] & B['H'], T1_ctrl['out2_L'])
- - - - - - - - - - - - - - - - - - - - - - - - - - - - - - - - - - - - - - -
ctrl.Rule(P['L'] & (B['L'] | B['M']), S1_ctrl['out2_L']),
ctrl.Rule(P['L'] & B['H'], S1_ctrl['out1_VL']),
ctrl.Rule(P['M'] & (V['L'] | V['H']) & (B['L'] | B['M']),
S1_ctrl['out3_LM']),
ctrl.Rule(P['M'] & (V['L'] | V['H']) & B['H'], S1_ctrl['out2_L']),
ctrl.Rule(P['M'] & V['M'] & (B['L'] | B['M']), S1_ctrl['out5_MH']),
ctrl.Rule(P['M'] & V['M'] & B['H'], S1_ctrl['out4_M']),
ctrl.Rule(P['H'] & V['L'] & (B['L'] | B['M']), S1_ctrl['out5_MH']),
ctrl.Rule(P['H'] & V['L'] & B['H'], S1_ctrl['out4_M']),
ctrl.Rule(P['H'] & V['M'] & (B['L'] | B['M']), S1_ctrl['out6_H']),
ctrl.Rule(P['H'] & V['M'] & B['H'], S1_ctrl['out5_MH']),
ctrl.Rule(P['H'] & V['H'] & (B['L'] | B['M']), S1_ctrl['out7_VH']),
ctrl.Rule(P['H'] & V['H'] & B['H'], S1_ctrl['out6_H'])
- - - - - - - - - - - - - - - - - - - - - - - - - - - - - - - - - - - - - - -
ctrl.Rule(V['L'] & P['L'] & (A['L'] | A['M']), T2_ctrl['out4_M']),
ctrl.Rule(V['L'] & P['L'] & A['H'], T2_ctrl['out5_MH']),
```

```
ctrl.Rule(V['L'] & P['M'] & (A['L'] | A['M']), T2_ctrl['out6_H']),
ctrl.Rule(V['L'] & P['M'] & A['H'], T2_ctrl['out7_VH']),
ctrl.Rule(V['L'] & P['H'], T2_ctrl['out7_VH']),
ctrl.Rule(V['M'] & (P['L'] | P['M']) & (A['L'] | A['M']),
T2_ctrl['out2_L']),
ctrl.Rule(V['M'] & (P['L'] | P['M']) & A['H'], T2_ctrl['out3_LM']),
ctrl.Rule(V['M'] & P['H'] & (A['L'] | A['M']), T2_ctrl['out4_M']),
ctrl.Rule(V['M'] & P['H'] & A['H'], T2_ctrl['out5_MH']),
ctrl.Rule(V['H'] & (P['L'] | P['M']), T2_ctrl['out1_VL']),
ctrl.Rule(V['H'] & P['H'] & (A['L'] | A['M']), T2_ctrl['out2_L']),
ctrl.Rule(V['H'] & P['H'] & A['H'], T2_ctrl['out3_LM']),
- - - - - - - - - - - - - - - - - - - - - - - - - - - - - - - - - - - - - - -
ctrl.Rule(V['L'] & (S['L'] | S['M']), S2_ctrl['out1_VL']),
ctrl.Rule(V['L'] & S['H'], S2_ctrl['out2_L']),
ctrl.Rule(V['M'] & (P['L'] | P['M']) & (S['L'] | S['M']),
S2_ctrl['out4_M']),
ctrl.Rule(V['M'] & (P['L'] | P['M']) & S['H'], S2_ctrl['out5_MH']),
ctrl.Rule(V['M'] & P['H'] & (S['L'] | S['M']), S2_ctrl['out3_LM']),
ctrl.Rule(V['M'] & P['H'] & S['H'], S2_ctrl['out4_M']),
ctrl.Rule(V['H'], S2_ctrl['out7_VH']).
```

The centroid defuzzification method was applied to complete the fuzzy modeling process for the controlled cleavage of silicate glasses, resulting in quantitative values for the output variables.

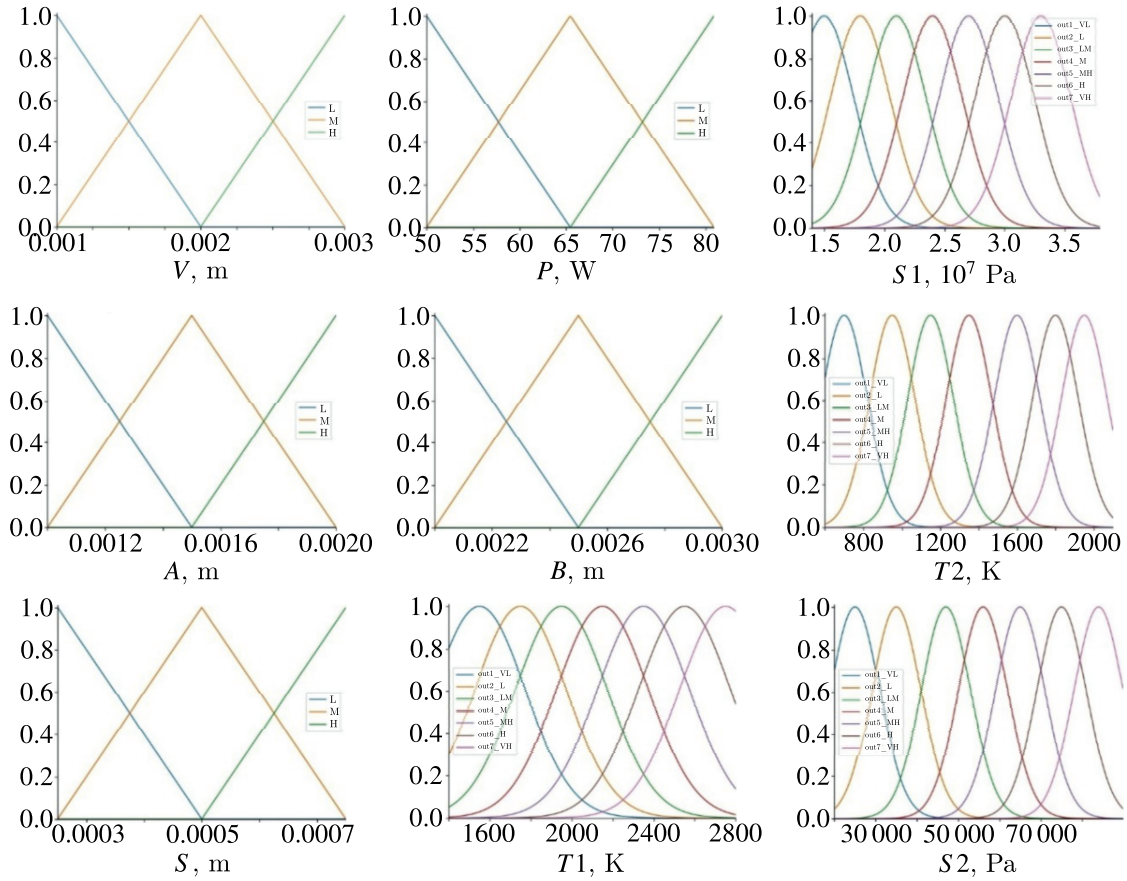

Figure 9. Membership functions of the linguistic variables for the input and output parameters

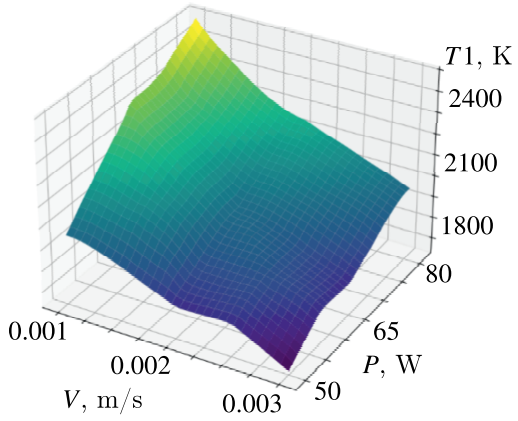

Figure 10. Maximum temperature $T1$ ($P6$) in the quartz plate at the end of laser treatment versus processing speed V ($P1$) and laser beam power, K

As an example, Fig. 10 presents the correlation between the maximum temperature $T1$ ($P6$) in the quartz glass plate at the end of the laser treatment and the processing speed, and laser beam power, as derived from the fuzzy model.

Neuro-fuzzy model

An Adaptive Neuro-Fuzzy Inference System (ANFIS) approach was applied to develop a predictive model capable of describing the relationships between the technological parameters of laser polishing and the resulting characteristics of the quartz glass laser processing. This method is characterized by its ability to hybridize the adaptive learning mechanisms of neural networks with the interpretable rule-based structure of fuzzy logic. The modeling was performed in the MATLAB environment using the Fuzzy Logic Toolbox and the ANFIS editor graphical interface, following the algorithm presented in Fig. 11 [Zhang, Lei, 2017].

The structure of the developed neuro-fuzzy model is predicated on a first-order Sugeno fuzzy inference system. Following data analysis and preliminary research, the subsequent network architecture was established: for each of the five input parameters V ($P1$), P ($P2$), A ($P3$), B ($P4$), S ($P5$), three Gaussian membership functions were assigned. This configuration automatically generated a fuzzy rule base consisting of 243 rules. The number of rules is determined by the grid structure; however, ANFIS is prone to overparameterization on limited datasets. Addressing this issue represents a promising direction for future research.

The neuro-fuzzy model was trained using data from the computational experiment (Table 1) with a hybrid optimization algorithm. This algorithm combines the least squares method for rapidly adjusting the parameters of the linear output rules and the gradient descent method for fine-tuning the parameters of the input membership functions. The rules were generated automatically using a first-order Sugeno fuzzy inference system, where the rule weights (consequent parameters) were tuned during the training process. The rule generation was based on a grid partitioning approach, involving an exhaustive search of all input term combinations.

As an example, Fig. 12 illustrates the relationship between the maximum temperature $T1$ ($P6$) in the quartz plate at the end of laser processing and the processing speed V ($P1$), and laser beam power P ($P2$), as predicted by the neuro-fuzzy model.

Neural network model

A feedforward neural network of the multilayer perceptron (MLP) type was implemented to describe the relationships between the input parameters of laser polishing V ($P1$), P ($P2$), A ($P3$),

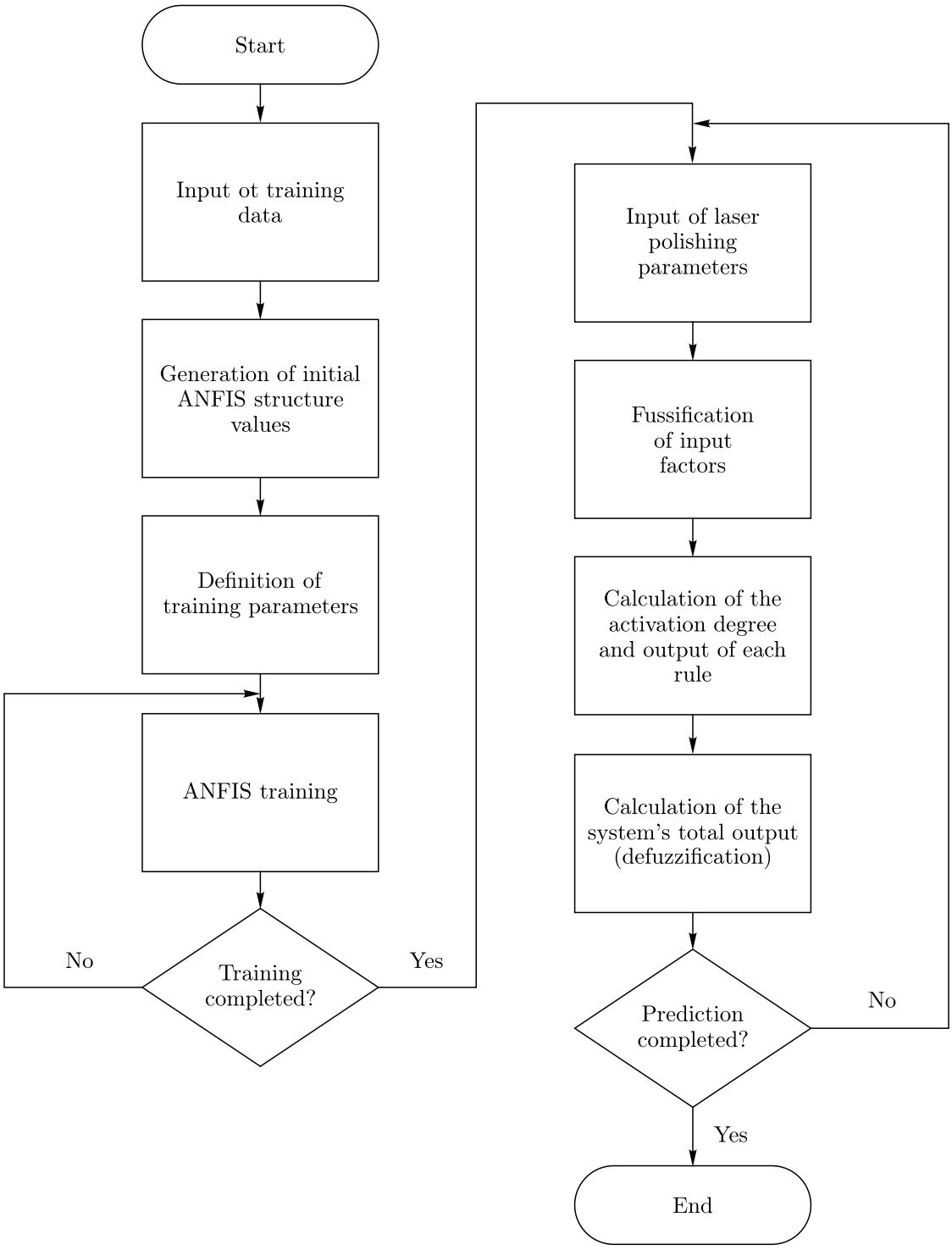

Figure 11. Neuro-fuzzy prediction process for laser polishing of fused quartz

B ($P4$), S ($P5$) and the output parameters $T1$ ($P6$), $S1$ ($P7$), $T2$ ($P8$), $S2$ ($P9$). This implementation utilized the TensorFlow 2.x library and the high-level Keras API, adhering to the algorithm presented in Fig. 13 [Головко, Краснопрошин, 2017; Nikityuk et al., 2022a].

During the development of the neural network, a Sequential model was used, consisting of the following layers. Input layer, defined by the input data dimensionality and comprising 5 neurons, which

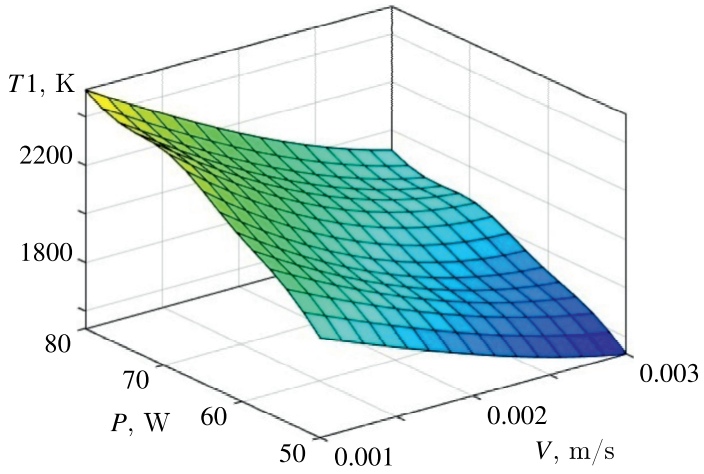

Figure 12. Maximum temperature $T1$ ($P6$) in quartz plate at the end of laser processing versus processing speed V ($P1$) and laser beam power P ($P2$)

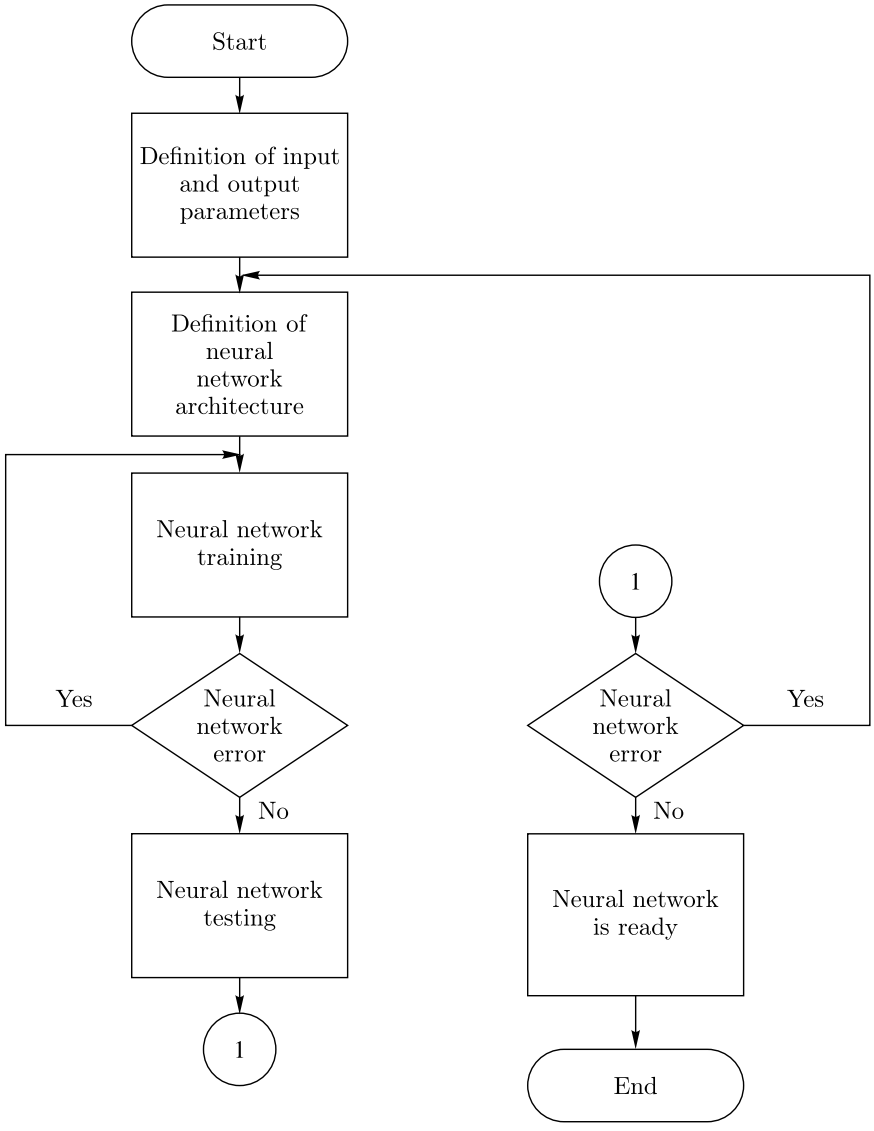

Figure 13. Flowchart of the neural network-based modeling process

corresponds to the number of input parameters. Two consecutive hidden fully-connected (Dense) layers. The activation function for neurons in both hidden layers is the Rectified Linear Unit (ReLU), selected for its effectiveness in preventing the vanishing gradient problem and high computational performance. The number of neurons in the first (nn1) and second (nn2) hidden layers was a variable parameter during the numerical experiments. Output fully-connected layer, consisting of 4 neurons, one for each predicted parameter. A linear activation function was used for this layer.

The model was compiled using the Adam optimizer, an efficient stochastic gradient optimization method with adaptive moment estimation. We employed the default learning rate (0.001) for the Adam optimizer, as it has proven to be robust across a diverse set of tasks. The mean squared error (MSE) was selected as the loss function. Each model was trained for 100 epochs.

A grid search was performed to determine the optimal architecture, focusing on two parameters: the number of neurons in the first (nn1) and second (nn2) hidden layers. Values of {5, 10, 15, 20, 25} were considered for each layer, resulting in 25 unique architectures in total.

The training and test datasets were generated by solving the corresponding problems using the finite element method in ANSYS software. The initial 27 combinations of the central composite experimental design were supplemented with an additional 100 computational combinations, ten of which were allocated to the test set (Table 2).

Table 2. Test dataset

No.	$P1$ (V), m/s	$P2$ (P), W	$P3$ (A), m	$P4$ (B), m	$P5$ (S), m	$P6$ ($T1$), K	$P7$ ($S1$), Pa	$P8$ ($T2$), K	$P9$ ($S2$), Pa
1	0.003	57	0.0015	0.00275	0.00025	1975	2.05E+07	1268	3.01E+04
2	0.0011	54	0.00175	0.0025	0.00075	2028	1.84E+07	1379	2.90E+04
3	0.0018	79	0.00125	0.0030	0.00075	2125	2.65E+07	1220	4.93E+04
4	0.0024	55	0.0015	0.00225	0.0005	1756	1.65E+07	811	6.96E+04
5	0.0025	63	0.00175	0.0025	0.00075	1804	1.94E+07	893	7.63E+04
6	0.0028	72	0.0015	0.00275	0.00075	1876	2.40E+07	898	8.27E+04
7	0.0018	77	0.00125	0.00225	0.00025	2256	3.00E+07	1205	4.35E+04
8	0.0014	73	0.0010	0.0030	0.0005	2173	2.45E+07	1322	3.06E+04
9	0.0019	59	0.00125	0.0020	0.00025	1994	2.63E+07	960	5.67E+04
10	0.0010	53	0.0015	0.00275	0.00025	2052	1.84E+07	1446	2.17E+04

The criteria outlined below were used to evaluate the resulting models:
Coefficient of determination:

$$R^2 = 1 - \frac{\frac{1}{n}\sum_{i=1}^{n}(d_i - y_i)^2}{\frac{1}{n}\sum_{i=1}^{n}(d_i - \overline{d})^2}.$$

Mean Absolute Error (MAE):

$$\mathrm{MAE} = \frac{1}{n}\sum_{i=1}^{n}|d_i - y_i|.$$

Root Mean Square Error (RMSE):

$$\mathrm{RMSE} = \sqrt{\frac{1}{n}\sum_{i=1}^{n}(d_i - y_i)^2}.$$

Mean Absolute Percentage Error (MAPE):

$$\text{MAPE} = \frac{1}{n}\sum_{i=1}^{n}\left|\frac{d_i - y_i}{d_i}\right| \cdot 100.$$

where d_i is the values obtained through the finite element method, y_i is the values predicted by the models.

To account for the explanatory variables that are less significant in the model, the adjusted coefficient of determination was used:

$$R_{adj} = 1 - \left(1 - R^2\right) \cdot \frac{n-1}{n-p-1},$$

where n represents the number of observations, and p denotes the quantity of input parameters.

Figure 14 provides four heatmaps, each corresponding to the MAPE (Mean Absolute Percentage Error) metric associated with one of the four output parameters: MAPE1 for $T1$, MAPE2 for $S1$, MAPE3 for $T2$, and MAPE4 for $S2$. The vertical and horizontal axes represent the number of neurons in the first and second hidden layers, respectively (ranging from 5 to 25 in increments of 5). The figure employs an inverted grayscale colormap, indicating that darker squares correspond to lower MAPE error values. Visual analysis shows that there is no single architecture that is absolutely the best for all four parameters. The optimal configuration depends on the specific target variable.

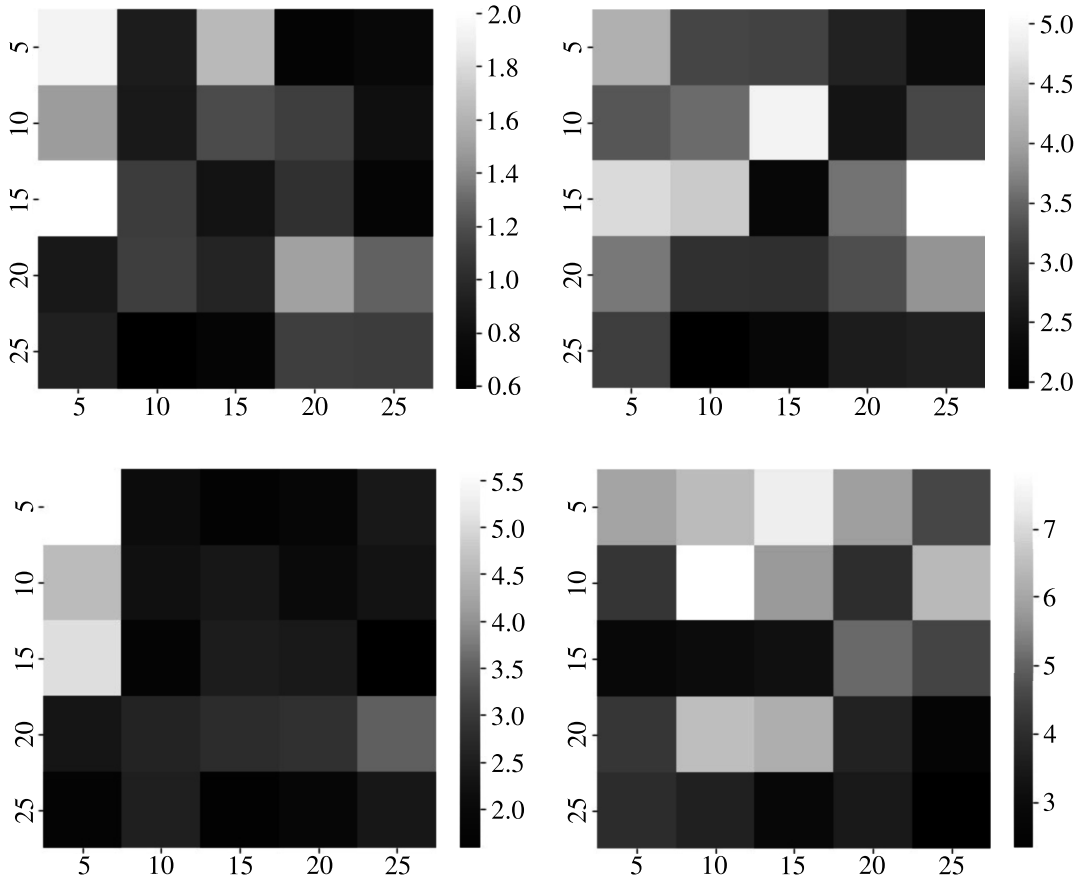

Figure 14. Heatmap of MAPE error distribution for predicting output parameters: (a) $T1$ ($P6$), (b) $S1$ ($P7$), (c) $T2$ ($P8$), (d) $S2$ ($P9$)

To identify the most universal architecture demonstrating the best-balanced results across all four output parameters, a ranking method based on all eight key metrics (MAPE and R^2_{Adj} for each of the four outputs) was used. As a result, the best-balanced model was determined to have an architecture with 25 neurons in the first hidden layer and 15 neurons in the second layer (25 × 15). This model demonstrated high and stable performance across all parameters.

Results and discussion

The quality of each model was evaluated on the test dataset using the following statistical metrics: Root Mean Square Error (RMSE), Mean Absolute Error (MAE), Mean Absolute Percentage Error (MAPE), Coefficient of Determination (R^2), and Adjusted Coefficient of Determination (R^2_{Adj}). The metric values for the regression, fuzzy, neuro-fuzzy, and neural network models are presented in Tables 3–6.

Table 3. Evaluation results of regression models

Statistical metric	Model response			
	*T*1 (*P*6)	*S*1 (*P*7)	*T*2 (*P*8)	*S*2 (*P*9)
RMSE	22	1.7E+06	11	4.0E+03
MAE	29	2.0E+06	13	4.5E+03
MAPE	1.1 %	8.2 %	1.0 %	9.1 %
R^2	0.9632	0.7659	0.9963	0.9524
R^2_{Adj}	0.9172	0.4732	0.9916	0.8929

Table 4. Evaluation results of neuro-fuzzy models

Statistical metric	Model response			
	*T*1 (*P*6)	*S*1 (*P*7)	*T*2 (*P*8)	*S*2 (*P*9)
RMSE	34	1.8E+06	70	3.1E+03
MAE	41	2.0E+06	90	3.4E+03
MAPE	1.7 %	8.3 %	5.9 %	7.8 %
R^2	0.9255	0.7614	0.8287	0.9735
R^2_{Adj}	0.8325	0.4633	0.6146	0.9403

Table 5. Evaluation results of fuzzy models

Statistical metric	Model response			
	*T*1 (*P*6)	*S*1 (*P*7)	*T*2 (*P*8)	*S*2 (*P*9)
RMSE	78	2.4E+06	121	6.7E+03
MAE	83	2.8E+06	130	7.5E+03
MAPE	3.9 %	11.5 %	11.0 %	18.0 %
R^2	0.6960	0.5414	0.6386	0.8671
R^2_{Adj}	0.5441	0.3121	0.4579	0.8007

A comparative analysis of the data presented in the tables demonstrates the superiority of the neural network model (MLP) over the other considered approaches. The neural network model shows the lowest error values (RMSE, MAE, MAPE) and the highest values of the coefficient of determination (R^2 and R^2_{Adj}) for all four output parameters. Additionally, the robustness of the neural network model

Table 6. Evaluation results of neural network models

Statistical metric	Model response			
	$T1$ ($P6$)	$S1$ ($P7$)	$T2$ ($P8$)	$S2$ ($P9$)
RMSE	13	4.8E+05	20	1.1E+03
MAE	16	6.6E+05	23	1.4E+03
MAPE	0.7 %	2.2 %	1.6 %	2.8 %
R^2	0.9890	0.9749	0.9885	0.9952
R^2_{Adj}	0.9752	0.9434	0.9742	0.9892

was evaluated using 5-fold cross-validation on the entire dataset. The averaged evaluation scores obtained further validated the results presented in Table 6.

This superiority is explained by the high capability of the MLP to approximate complex, nonlinear, and implicit dependencies between the technological parameters and the final quality characteristics, which are not fully captured by polynomial regression or rule-based fuzzy systems. It should be noted that a larger amount of data was used to create the quartz glass laser polishing model compared to the other models. These high accuracy and explanatory power confirm that the developed neural network model serves as a reliable predictive tool.

Determination of optimal parameters for the laser polishing process of quartz plates

The development of a sufficiently accurate neural network model, as described in the previous section, serves not only as a tool for process analysis but also as a foundation for solving the problem of identifying optimal technological conditions for laser polishing.

Determination of these conditions manually or by enumeration is inefficient due to the multidimensional nature of the input parameter space and complex nonlinear interrelationships. To solve this multiobjective optimization problem, a genetic algorithm implemented in Python [Nikitjuk, Serdyukov, 2023] was applied. This algorithm utilized the previously trained and saved neural network with the [5-25-15-4] architecture as a surrogate model.

The optimization objective was to find a set of controllable input parameters {V ($P1$), P ($P2$), A ($P3$), B ($P4$), S ($P5$)} that provides the optimal balance between processing efficiency and quality while adhering to technological constraints.

Target (optimized) parameters were set as follows: maximization of processing speed: $V \to \max$, and minimization of residual von Mises equivalent stress $S2$ ($P9$): $S2 \to \min$.

Process constraints required the maximum temperature in the processing zone $T1$ ($P6$) to remain within $2273 \leqslant T1 \leqslant 2323$ K.

Controlled (input) parameters and their search ranges were defined as follows: speed V: [0.001, 0.003] m/s, power P: [50, 80] W, semiaxis A: [0.001, 0.002] m, semiaxis B: [0.002, 0.003] m, scanning pitch S: [0.00025, 0.00075] m.

To solve the presented multiobjective optimization problem, a scalarization method was employed, which reduces multiple criteria to a single fitness value. The objective function L, which the genetic algorithm aims to minimize, was constructed following the approach outlined in [Nikitjuk, Serdyukov, 2023] and includes both the optimization targets and penalty terms for any constraint violations:

$$L(V, P, A, B, S) = -(\alpha_1 V - \alpha_2 S2) + \sum_{i=1}^{6} \beta_i E_i,$$

where

$$E_1 = \begin{cases} 1 & \text{if } 0.001 > V > 0.003 \text{ m/s}, \\ 0 & \text{if } 0.001 \leqslant V \leqslant 0.003 \text{ m/s}; \end{cases} \qquad E_2 = \begin{cases} 1 & \text{if } 50 > P > 80 \text{ W}, \\ 0 & \text{if } 50 \leqslant P \leqslant 80 \text{ W}; \end{cases}$$

$$E_3 = \begin{cases} 1 & \text{if } 0.001 > A > 0.002 \text{ m}, \\ 0 & \text{if } 0.001 \leqslant A \leqslant 0.002 \text{ m}; \end{cases} \qquad E_4 = \begin{cases} 1 & \text{if } 0.002 > B > 0.003 \text{ m}, \\ 0 & \text{if } 0.002 \leqslant B \leqslant 0.003 \text{ m}; \end{cases}$$

$$E_5 = \begin{cases} 1 & \text{if } 0.00025 > S > 0.00075 \text{ m}, \\ 0 & \text{if } 0.00025 \leqslant S \leqslant 0.00075\text{m}; \end{cases} \qquad E_6 = \begin{cases} 0 & \text{if } 2273 > T1 > 2323 \text{ K}, \\ 1 & \text{if } 2273 \leqslant T1 \leqslant 2323 \text{ K}; \end{cases}$$

$$\alpha_1 = \alpha_2 = 0.5, \quad \beta_i = 1.0, \quad i = \overline{1, 6}.$$

The evolutionary process incorporated tournament selection, single-point crossover, and mutation. The algorithm termination conditions were set at reaching 200 iterations or if the best solution showed no improvement over 50 consecutive iterations. The multiobjective optimization process using the genetic algorithm was executed with a population size of 500 individuals.

Figure 15 shows the algorithm's convergence dynamics, displaying the "raw" fitness values (excluding penalties) for the best individual (solid line) and the average value across the population (dashed line) in each generation.

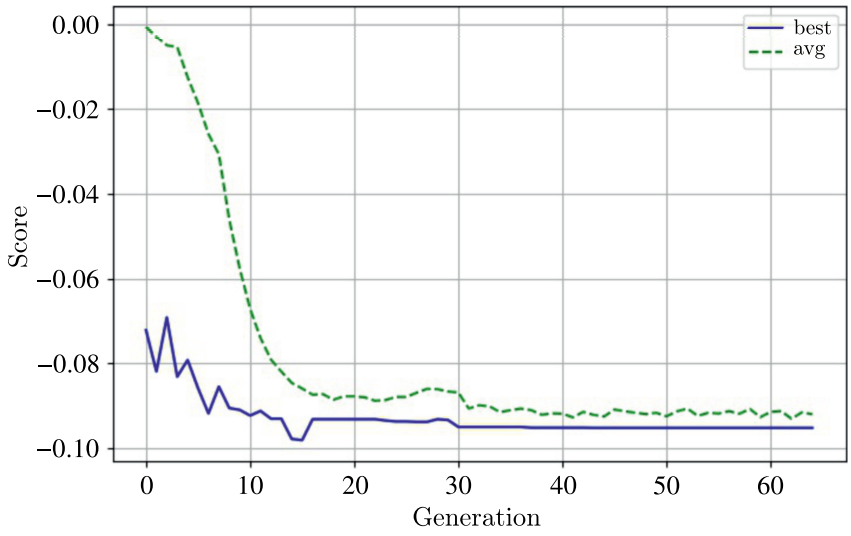

Figure 15. Convergence process of the genetic algorithm for solving the multiobjective optimization problem of laser polishing parameters for quartz plates

The graph analysis reveals that rapid convergence occurs during the initial phase (generations 0–15). The average population fitness (avg) markedly enhances (the value drops from 0 to −0.09) as the algorithm quickly eliminates inefficient random solutions. Concurrently, an active search for the best solution (best) occurs, which also shows substantial enhancement. Starting approximately from generation 15, the algorithm enters a stabilization phase. The average population fitness reaches a plateau, indicating the achievement of a high overall quality in the gene pool. The best solution also stabilizes at a value of approximately −0.098, suggesting the discovery of a global or sufficiently deep local optimum within the search space. As evident from the algorithm's operation log, starting from generation 20 onwards, the best-found solution no longer improved, which ultimately triggered the early stopping criterion.

The algorithm's execution resulted in an optimal combination of technological parameters that fully satisfies the specified temperature constraints and provides the best compromise between processing efficiency and quality. The optimization results are presented in Table 7.

Table 7. Results of multiobjective optimization

No.	*P*1 (*V*), m/s	*P*2 (*P*), W	*P*3 (*A*), m	*P*4 (*B*), m	*P*5 (*S*), m	*P*6 (*T*1), K	*P*7 (*S*1), Pa	*P*8 (*T*2), K	*P*9 (*S*2), Pa
1	0.0017	79	0.0016	0.0026	0.0004	2283 (2225)	2.75E+07 2.78E+07	1306 (1342)	3.93E+04 (3.77E+04)

The values in parentheses represent the parameters derived from finite element modeling of the laser polishing process applied to the quartz plate, using the optimal factor values identified through the genetic algorithm. The established output parameters demonstrate that the errors do not exceed 5 %.

Conclusion

The study presents a comprehensive analysis and modeling of the fused quartz laser polishing process, aiming to develop effective tools for predicting its key characteristics.

In the first stage, a finite element model was developed and verified, accurately describing the distribution of temperature and stress in the material under CO_2 laser exposure. From the data obtained during the computational experiment, four predictive models were constructed and analyzed: regression, fuzzy logic, neuro-fuzzy, and neural network models.

The comparative analysis revealed that, while regression and ANFIS models can describe the general trends of the process with acceptable accuracy, they are somewhat limited in their ability to capture the full complexity of the nonlinear relationships between the technological parameters of quartz glass laser polishing. The highest performance was demonstrated by the multilayer perceptron (MLP) neural network model. Owing to its flexible architecture and training on an extended dataset, this model achieved superior predictive accuracy across all output parameters, as confirmed by adjusted coefficient of determination values exceeding 0.97 and a mean absolute percentage error below 3 %.

An important phase of the research involved applying the developed neural network model to determine the optimal technological conditions for laser polishing of fused quartz. A genetic algorithm was employed for this purpose, utilizing the neural network as a surrogate model for rapid fitness evaluation. The genetic algorithm successfully identified an optimal combination of technological parameters that fully satisfies the specified temperature constraints and achieves the best compromise between processing efficiency and quality. For verification, the optimization results were validated using finite element modeling, which confirmed the high predictive accuracy of the neural network model, i. e., the error for output parameters did not exceed 5 %.

Thus, methods involving artificial intelligence, particularly neural networks, represent a powerful and effective tool for modeling and optimizing complex technological processes. Overall, the resulting models and the optimization approach can be applied to select optimal processing parameters, minimize experimental efforts, and develop intelligent control systems for technological processes.

References

Арбузов В. И. Основы радиационного оптического материаловедения. — СПб.: СПбГУ ИТМО, 2008. — 284 с.

Arbuzov V. I. Osnovy radiatsionnogo opticheskogo materialovedeniya [Fundamentals of radiation optical materials science]. — Saint Petersburg: SPbGU ITMO, 2008. — 284 p. (in Russian).

Бибичева С. А., Рупасов А. Е., Данилов П. А., Ионин А. А., Смирнов Н. А., Кудряшов С. И., Шелыгина С. Н., Заколдаев Р. А. Самоорганизующиеся субволновые периодические решетки на поверхности кварцевого стекла // Оптика и спектроскопия. — 2022. — Т. 130, вып. 4. — С. 555–558. — https://doi.org/10.21883/os.2022.04.52272.58-21

Bibicheva S. A., Rupasov A. E., Danilov P. A., Ionin A. A., Smirnov N. A., Kudryashov S. I., Shelygina S. N., Zakoldaev R. A. Samoorganizuyushchiesya subvolnovye periodicheskie reshetki na poverhnosti kvarcevogo stekla [Self-organizing subwavelength periodic lattices on the surface of quartz glass] // Optika i spektroskopiya. — 2022. — Vol. 130, No. 4. — P. 555-558. — https://doi.org/10.21883/os.2022.04.52272.58-21 (in Russian).

Головко В. А., Краснопрошин В. В. Нейросетевые технологии обработки данных: учебное пособие. — Минск: БГУ, 2017. — 263 с.

Golovko V. A., Krasnoproshin V. V. Neyrosetevye tekhnologii obrabotki dannykh: uchebnoe posobie [Neural network technologies for data processing: textbook]. — Minsk: BGU, 2017. — 263 p. (in Russian).

Достанко А. П., Аваков С. М., Голосов Д. А., Емельянов Е. В., Завадский С. М., Колос В. В., Ланин В. Л., Мадвейко С. И., Мельников С. Н., Никитюк Ю. В., Петлицкий А. Н., Петухов И. Б., Пилипенко В. А., Плебанович В. И., Солодуха В. А., Соколов С. И., Телеш Е. В., Шершнев Е. Б. Инновационные технологии и оборудование субмикронной электроники / под ред. акад. НАН Беларуси А. П. Достанко. — Минск: Беларуская навука, 2020. — 260 с.

Dostanko A. P., Avakov S. M., Golosov D. A., Emel'yanov E. V., Zavadskii S. M., Kolos V. V., Lanin V. L., Madveiko S. I., Mel'nikov S. N., Nikityuk Yu. V., Pelitskii A. N., Petuhov I. B., Pilipenko V. A., Plebanovich V. I., Soloduha V. A., Sokolov S. I., Telesh E. V., Shershnev E. B. Innovatsionnye tekhnologii i oborudovanie submikronnoy elektroniki [Innovative technologies and equipment for submicron electronics] / pod red. A. P. Dostanko. — Minsk: Belaruskaya navuka, 2020. — 260 p. (in Russian).

Емельянов В. А., Шершнев Е. Б., Никитюк Ю. В., Соколов С. И., Аушев И. Ю. Оптимизация лазерной полировки кварцевого стекла с использованием метода планирования вычислительных экспериментов // Проблемы физики, математики и техники. — 2022. — № 2 (51). — С. 26–30. — DOI: 10.54341/20778708_2022_2_51_26

Emelyanov V. A., Shershnev E. B., Nikityuk Yu. V., Sokolov S. I., Aushev I. Yu. Optimizatsiya lazernoy polirovki kvartsovogo stekla s ispol'zovaniem metoda planirovaniya vychislitel'nykh eksperimentov [Optimization of laser polishing of quartz glass using the method of planning computational experiments] // Problemy fiziki, matematiki i tekhniki. — 2022. — No. 2 (51). — P. 26–30. — DOI: 10.54341/20778708_2022_2_51_26 (in Russian).

Марченко Л. Н., Косенок Я. А., Гайшун В. Е., Бруттан Ю. В. Моделирование реологических характеристик водных суспензий на основе наноразмерных частиц диоксида кремния // Компьютерные исследования и моделирование. — 2024. — Т. 16, № 5. — С. 1217–1252. — DOI: 10.20537/2076-7633-2024-16-5-1217-1252

Marchanko L. N., Kasianok Ya. A., Gaishun V. E., Bruttan I. V. Modeling of rheological characteristics of aqueous suspensions based on nanoscale silicon dioxide particles // Computer Research and Modeling. — 2024. — Vol. 16, No. 5. — P. 1217–1252. — DOI: 10.20537/2076-7633-2024-16-5-1217-1252 (in Russian).

Никитюк Ю. В., Васильев А. Ф., Марченко Л. Н., Ма Ц., Ван Л., Цинь Ю., Аушев И. Ю. Определение параметров управляемого лазерного раскалывания силикатных стекол с использованием регрессионных, нейросетевых и нечетких моделей // Проблемы физики, математики и техники. — 2024. — № 2 (59). — С. 32–38.

Nikityuk Yu. V., Vasiliev A. F., Marchenko L. N., Ma Ts., Van L., Tsin' Yu., Aushev I. Yu. Opredelenie parametrov upravlyaemogo lazernogo raskalyvaniya silikatnykh stekol s ispol'zovaniem regressionnykh, neyrosetevykh i nechetkih modeley [Determination of parameters of controlled laser splitting of silicate glasses using regression, neural network, and fuzzy models] // Problemy fiziki, matematiki i tekhniki. — 2024. — No. 2 (59). — P. 32–38 (in Russian).

Никитюк Ю. В., Прохоренко В. А., Кулыба А. И. Многокритериальная оптимизация параметров лазерной резки кварцевого стекла с применением нейросетевого моделирования и генетического алгоритма // Проблемы физики, математики и техники. — 2023. — № 3 (56). — С. 26–31.

Nikityuk Yu. V., Prokhorenko V. A., Kulyba A. I. Mnogokriterial'naya optimizatsiya parametrov lazernoy rezki kvartsovogo stekla s primeneniem neyrosetevogo modelirovaniya i geneticheskogo algoritma [Multicriteria optimization of laser cutting parameters for quartz glass using neural network modeling and genetic algorithm] // Problemy fiziki, matematiki i tekhniki. — 2023. — No. 3 (56). — P. 26–31 (in Russian).

Сердюков А. Н., Шершнев Е. Б., Никитюк Ю. В., Шолох В. Ф., Соколов С. И. Особенности управляемого лазерного термораскалывания кристаллического кварца // Кристаллография. — 2012. — Т. 57, № 6. — С. 879–885.

Serdyukov A. N., Shershnev E. B., Nikityuk Yu. V., Sholoh V. F., Sokolov S. I. Osobennosti upravlyaemogo lazernogo termoraskalyvaniya kristallicheskogo kvarca [Features of controlled laser thermal cleavage of crystalline quartz] // Kristallografiya. — 2012. — Vol. 57, No. 6. — P. 879–885 (in Russian).

Шершнев Е. Б., Никитюк Ю. В., Шершнев А. Е., Соколов С. И. Исследование процесса лазерной полировки кварцевого стекла // Проблемы физики, математики и техники. — 2015. — № 4 (25). — С. 45–49.
Shershnev E. B., Nikityuk Yu. V., Shershnev A. E., Sokolov S. I. Issledovanie protsessa lazernoy polirovki kvartsovogo stekla [Investigation of the laser polishing process of quartz glass] // Problemy fiziki, matematiki i tekhniki. — 2015. — No. 4 (25). — P. 45–49 (in Russian).

Штовба С. Д. Проектирование нечетких систем средствами MATLAB. — М.: Горячая линия – Телеком, 2007. — 284 с.
Shtovba S. D. Proektirovanie nechetkih sistem sredstvami MATLAB [Design of fuzzy systems using MATLAB]. — Moscow: Goryachaya liniya – Telekom, 2007. — 284 p. (in Russian).

Hildebrand J., Hecht K., Bliedtner J., Müller H. Advanced analysis of laser beam polishing of quartz glass surfaces // Physics Procedia. — 2012. — Vol. 39. — P. 277–285. — DOI: 10.1016/j.phpro.2012.10.039

Hildebrand J., Hecht K., Bliedtner J., Müller H. Laser beam polishing of quartz glass surfaces // Physics Procedia. — 2011. — Vol. 12. — P. 452–461. — DOI: 10.1016/j.phpro.2011.03.057

Jiang P., Zhou Q., Shao X. Surrogate model-based engineering design and optimization. — Singapore: Springer, 2020. — 240 p. — DOI: 10.1007/978-981-15-0731-1_8

Kanevskii V., Fu H., Kolienov S., Grygoruk V., Zhang H., Stelmakh O. Theoretical analysis of nanoscale local etching of a rough quartz surface under direct illumination // Optics Express. — 2024. — Vol. 32, No. 14. — P. 24728-24743. — https://doi.org/10.1364/oe.518668

Kharche P. P., Patil V. H. Systematic review of optimization techniques for laser beam machining // Engineering Research Express. — 2024. — Vol. 6, No. 2. — P. 213–219. — DOI: 10.1088/2631-8695/ad594b

Lu G., Zhang Y., Lei J. Process parameter optimization for CO2 laser polishing of fused silica using the Taguchi method // Materials. — 2024. — Vol. 17, No. 3. — P. 709. — DOI: 10.3390/ma17030709

Mohajerani S., Bordatchev E., Tutunea-Fatan O. Recent developments in modeling of laser polishing of metallic materials // Lasers Manuf. Mater. Process. — 2018. — Vol. 5. — P. 395–429. — https://doi.org/10.1007/s40516-018-0071-5

Nikityuk Y., Prokhorenko V., Semchenko A., Kovalenko D. Optimization of quartz Sol-Gel glass cutting parameters by elliptical laser beams using neural network simulation and genetic algorithm // Recent Advances in Technology Research and Education. Inter-Academia 2023. Lecture Notes in Networks and Systems. — Cham: Springer, 2024. — Vol. 939. — P. 343–350. — DOI: 10.1007/978-3-031-54450-7_34

Nikitjuk Y., Serdyukov A. Determination of the parameters of controlled laser thermal cleavage of crystalline silicon using regression and neural network models // Crystallography Reports. — 2023. — Vol. 68, No. 7. — P. 195–200.

Nikityuk Y., Serdyukov A., Aushev I. Optimization of two-beam laser cleavage of silicate glass // Journal of Optical Technology. — 2022a. — Vol. 89, No. 2. — P. 121–125.

Nikitjuk Y. V., Serdyukov A. N., Aushev I. Y. Determination of the parameters of two-beam laser splitting of silicate glasses using regression and neural network models // Journal of the Belarusian State University. Physics. — 2022b. — No. 1. – P. 35–43. — DOI: 10.33581/2520-2243-2022-1-35-43

Nikityuk Yu. V., Sereda A. A., Serdyukov A. N. Laser cleaving of brittle non-metallic materials. — Gomel: Francisk Skorina Gomel State University, 2025. — 217 p.

Nisar S. Optimization of laser beam geometry for controlling thermal stresses in CO_2 laser glass cutting // Lasers in Manufacturing and Materials Processing. — 2025. — Vol. 12, No. 2. — P. 298–317. — DOI: 10.1007/s40516-025-00289-6

Rosa B., Hascoet J. Y., Mognol P. Modeling and optimization of laser polishing process // Applied Mechanics and Materials. — 2014. — Vol. 575. — P. 766–770. — https://doi.org/10.4028/www.scientific.net/amm.575.766

Serdyukov A. N., Shalupaev S. V., Nikityuk Y. V. Features of controlled laser thermal cleavage of crystalline silicon // Crystallography Reports. — 2010. — Vol. 55, No. 6. — P. 933–937. — DOI: 10.1134/S1063774510060064

Serdyukov A. N., Shershnev E. B., Nikityuk Y. V., Sholokh V. F., Sokolov S. I. Features of controlled laser thermal cleavage of crystal quartz // Crystallography Reports. — 2012. — Vol. 57, No. 6. — P. 792–797. — DOI: 10.1134/S1063774512060120

Solheid J. S., Elkaseer A., Wunsch T., Scholz S., Seifert H. J., Pfleging W. Multiobjective optimization of laser polishing of additively manufactured Ti-6Al-4V parts for minimum surface roughness and heat-affected zone // Materials. — 2022. — Vol. 15. — P. 3323. — https://doi.org/10.3390/ma15093323

Sysoev V. K. Laser etching and polishing of quartz tubes // Glass and Ceramics. — 2003. — Vol. 60, No. 7–8. — P. 223–226.

Zhang Y., Lei J. Prediction of laser cutting roughness in intelligent manufacturing mode based on ANFIS // Procedia Engineering. — 2017. — Vol. 174. — P. 82–89. — DOI: 10.1016/j.proeng.2017.01.149